Proceedings of ASME Turbo Expo 2019: Turbomachinery Technical Conference and Exposition
GT2019
June 17-21, 2019, Phoenix, Arizona, USA

GT2019-91817

COMPARISON OF THIN FILM HEAT FLUX GAUGE TECHNOLOGIES EMPHASIZING CONTINUOUS-DURATION OPERATION

Shawn Siroka, Reid A. Berdanier, Karen A. Thole
The Pennsylvania State University
University Park, PA, USA

Kam S. Chana
Oxford University
Oxford, UK

Charles W. Haldeman
Pratt & Whitney
East Hartford, CT, USA

Richard J. Anthony
Air Force Research Laboratory
WPAFB, OH, USA

ABSTRACT

Thin film heat flux gauges (HFGs) have been used for several decades to measure surface temperatures and heat flux in test turbines with the majority being used in facilities that are short-duration. These gauges are typically composed of two resistive temperature devices deposited on opposing sides of a dielectric. However, because these sensors have been traditionally applied for measurements in short-duration, transient-type facilities, the challenges facing adaptation of this technology for a continuous-duration steady facility warrant investigation. Those challenges are highlighted, and solutions are presented throughout the paper. This paper describes the nanofabrication process for heat flux gauges and a new calibration method to address potential deterioration of gauges over long runtimes in continuous-duration facilities. Because a primary uncertainty of these sensors arises from the ambiguity of the thermal properties, special emphasis is placed on the property determination and potential errors due to improper thermal properties. Also, this paper presents a discussion on the use of impulse response theory to process the data showing the feasibility of the method for steady-duration facilities after an initial settling time. The latter portion of the paper focuses on comparing well-established heat flux gauges developed for short-duration turbine test facilities to recently developed gauges fabricated using modern nanofabrication techniques for a continuous turbine test facility. Using a commercially available heat flux gauge, capable of measuring a steady heat flux as a reference, the gauges were compared using the test case of an impinging jet over a range of Reynolds numbers. The comparison between the PSU gauge and the reference device indicated agreement within 14%, and similar results were achieved through comparison with established sensors from partner institutions.

NOMENCLATURE

b	Resistive element half width
c_p	Specific heat
d	Thickness
D	Diameter
H	Spacing from impingement jet, H = 4D
I	Current
k	Thermal conductivity
L	Length of heater
Pt	Platinum
q	heat flux
q'	wave number = i/ λ
Q	Sinusoidal heat flux
R	Resistance
Re_D	Reynolds number, $Re_D = U \cdot D \cdot \nu^{-1}$
T	Static temperature
t	Time
V	Voltage

Greek

α	Linear coefficient of thermal expansion
β	Coefficient of resistance
ε	Percent error
ϵ	3-omega constant = 0.922
Δ	Change in quantity
λ	Thermal wavelength
ρ	Density
ω	Excitation frequency for 3-omega method
ϖ	Frequency of boundary condition for IRT method

Subscripts

0	Peak amplitude value
ref	Reference Temperature
3ω	Amplitude of the third harmonic of ω
h	Heater
bot	Bottom side of heat flux gauge
mean	Average value

op	Evaluated at operating condition
prop	Thermal property evaluation condition
top	Top side of heat flux gauge

INTRODUCTION

For nearly four decades, thin film heat flux gauges (HFGs) have been used to quantify heat transfer metrics for turbine components. Initial development of these sensors for turbomachinery was led concurrently by Oxford University [1,2] and MIT [3]. In the years that followed, this technology expanded to other institutions, including The Ohio State University [4] the von Karman Institute (VKI) [5], Virginia Tech [6], and the U.S. Air Force Research Laboratory (AFRL) [7,8]. For each of these users, the HFGs are applied in short-duration, blow-down tests with total operating times on the order of seconds or less. In contrast, continuous-duration facilities operate with time scales of hours and days pose potential challenges for installation and operation of HFGs as well as post processing.

This disparity of run times is illustrated in Table 1 showing a representative single-test run time for each facility. Using these run times, a worst-case scenario is calculated assuming three tests per day operating 365 days per year over a period of 20 years. For many of these facilities, a cumulative 20-year test time is on the order of a few hours, a period which will easily be overcome in a single test day for a continuous-duration facility such as the Steady Thermal Aero Research Turbine (START) facility at the Pennsylvania State University. In reality, most of these test articles can only operate one or two tests per day over a maximum of about four days per week, therefore further widening the gap.

This paper focuses on understanding the challenges associated with implementing HFGs in a continuous-duration facility and presenting viable solutions. A new *in situ* calibration procedure is evaluated, and the influence of thermal properties on calculated parameters is assessed. For these cases, an impulse response filter is used and considered for use in continuous-duration conditions. Finally, tests conducted with sensors manufactured at the Nanofabrication Lab at Penn State are compared with a commercially-available Heat Flux Microsensor (HFM) as well as established gauges currently in use at Oxford and AFRL.

Table 1: Comparison of HFGs in a Range of Rotating Facilities

Facility	Ref	Length of Test [s]	Tests/Day	Cumulative 20 Year Test Time [hrs]
Ohio State TTF	[9]	0.120	3	0.730
MIT	[10]	0.200	3	1.217
Oxford ORF	--	0.200	3	1.217
Oxford OTRF	--	0.500	3	3.042
VKI	[11]	0.500	3	3.042
AFRL	--	2.500	3	15.208
Virginia Tech	[6]	25.000	3	152.08
Penn State	--	8 [hrs]	1	58,400

BACKGROUND

Epstein et al. [3,10] outlined the theory for double-sided heat flux gauges, followed by other practical studies on mid-span turbine heat transfer using the instrumentation with numerical post processing schemes [12,13]. Since then, this technology has enabled the study of unsteady heat flux for turbine components in both the stationary [5,14,15] and rotating [15,16] reference frame of airfoils, in the tip region [18–20], and more, benefitting from a minimally-intrusive design. Different types have been used [21–24], but all operate by solving the unsteady conduction equation through a substrate or substrates given a set of boundary conditions.

These boundary conditions can be obtained in two different ways. For example, a single-sided gauge, as seen in Figure 1(a) solves the conduction equation using one measured temperature and applying a semi-infinite approximation. In contrast, a double-sided thin film heat flux sensor, Figure 1(b), has a temperature measuring device on both sides of a known substrate.

A double-sided thin film heat flux sensor must be used when operating in steady conditions because the backside boundary condition cannot be treated as semi-infinite. By adding the second sensor, one can always measure the heat flux because the backside boundary condition is measured. This property makes it the right choice for a steady facility. To measure heat flux accurately, there must be a measurable temperature difference across the substrate. Because the substrate is inherently thin for this type of sensor, large heat fluxes are necessary to create a temperature difference discernable from the uncertainty in the measurement. For the START Lab, this large heat flux comes from actively cooling the part which creates an expected gas-to-metal temperature ratio of 1.3 K/K found from CFD predictions.

Although other types exist, the focus of this study is on single- and double-sided thin film HFGs where the dielectric beneath the temperature sensing element is polyimide. This limited scope is due to the way in which the instruments have been used in the past and will be first used in the START facility. However, as sensor fabrication becomes ever more intricate (such as direct deposition to an airfoil [25]) the solutions in this paper to the challenges in adapting heat flux gauges to a steady measurement will still hold.

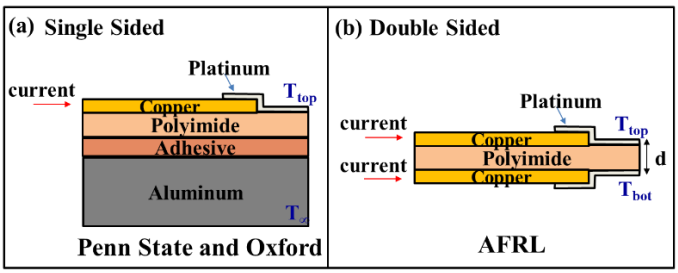

Figure 1: Typical heat flux gauge designs: (a) single-sided, (b) double-sided.

To obtain the temperatures required to solve the unsteady conduction equation, thin-film resistive temperature devices (RTDs) are often implemented. To create these sensors, manual application of platinum paint may be used, but lithography processes can significantly improve control of dimensionality and alignment for double-sided gauges. A lithography technique typically requires advanced equipment, but has been used to

successfully execute gauge designs using nickel [3,26] and platinum [5,27,28] resistive elements.

Beyond sensor fabrication, material properties of the dielectric must be precisely known to achieve accurate calculated results. This study focuses on a polyimide due to its dimensional stability, dielectric properties, and flexibility, but other materials such as quartz [29] and Macor [30] have been used in the past. Most important, it has been previously identified that the bulk thermal properties for polyimide substrates provided by the manufacturer can vary by as much as 20% from the measured value, and therefore must be independently validated [3].

In some cases, previous studies have empirically quantified these thermal properties as lumped parameters, specifically $\sqrt{\rho c_p k}$ and k/d [24]. As one example of this method, a known heat flux can be introduced to the HFG, and the sensor response can be used to deduce the parameters of interest. Unfortunately, identifying a viable heat flux source can be difficult. Past studies have used an oil bath [26], a laser [3], and even the resistive element itself as the heater [31]. However, many authors have converged on a heated air gun serving as an impinging jet on the gauge for its repeatability and accurate representation of convective experimental conditions [24,26,32].

FABRICATION

Within Penn State's Nanofabrication Lab, a process was developed to produce single- and double-sided HFGs with high yield and repeatable results. The workflow is similar to that presented by Collins et al. [28]. Following this process, the gauges were manufactured through a combination of subtractive and additive processes, starting with a sheet of Pyralux®, a commercially-available product comprising a polyimide sheet with 9 μm of copper on each side. In the first part of the fabrication process, copper is removed from the Pyralux through an etching process, creating the pattern for the lead wires. The substrate then goes through a patterning process involving a mask for the platinum elements. Platinum is then deposited through an evaporative physical vapor deposition process, which differentiates this process from Collins et al. [28], where the platinum was sputtered. The platinum bridges the two lead wires and functions as the RTD element.

After completing these steps, a similar process is completed on the opposite side of the substrate. Penn State's capabilities enable front and back side feature alignment within 5 μm. Through an application of the latest nanofabrication techniques, this alignment capability represents a new standard for HFG fabrication, a factor of two improvement over original manufacturing guidelines reported by Epstein et al. [10].

Accurate alignment capability is important for an orthogonal one-dimensional (1D) heat flux assumption to hold. Because the metal temperature is not a fixed parameter in the START turbine, large spatial gradients of temperature across the part could lead to a breakdown of the 1D assumption for these gauges. By ensuring the gauges are aligned to within 5 μm (5% of the smallest geometrical dimension for the present design), the heat flux can be treated as one dimensional and orthogonal to the airfoil surface.

Figure 2 compares the design intent to the fabricated gauge for sensors manufactured at Penn State. Because the physical vapor deposition process is more precise than the etching process, the dimensionality of the platinum is more controlled than the copper (as identified by a slight overhang of platinum on the top portion of the gauge). Although these gauges represent a sensing element 90 μm x 500 μm, gauges with features as small as 4 μm have been successfully fabricated at Penn State. Controlling the geometry and the amount of platinum deposited changes the resistance of the sensor. After the fabrication is complete, the sensor must be calibrated before it can be used.

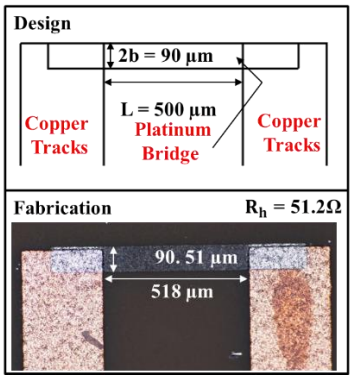

Figure 2: Comparison of HFG design-intent with as-built geometry.

CALIBRATION

Traditionally, the calibration process has been performed using a calibration bath. This study evaluates a standard calibration bath process and expands the calibration procedures by proposing the feasibility of another technique called the 3-omega method, which enables continuous-duration facilities to routinely check HFG calibration coefficients.

Oil Bath Calibration

Because platinum has a linear resistance behavior over the temperatures of interest, the calibration curve is dependent upon the offset and the slope of the fit. The offset is the reference resistance and the slope of the line is the coefficient of resistance. For this study, a temperature calibration bath was used with silicone oil as the heat transfer fluid. The bath has a uniformity to within 0.02°C and a stability within 0.01°C. A higher degree of accuracy was achieved by pairing the bath with a reference thermometer and an RTD, ultimately yielding an overall accuracy of 0.05°C.

Before the calibration procedure begins, gauges were annealed at a fixed temperature, slightly higher than the expected maximum operating temperature of the sensor, until the nominal resistance of the gauges changed by less than 1% over an hour. This step is necessary to relax the internal stresses in the gauge left during the evaporative deposition process and mitigate hysteresis in thermal properties.

Next, the calibration bath was automatically swept through the predefined temperature calibration range and repeated several times to quantify hysteresis; typical results are shown in Figure 3. The calibration measures the voltage drop across the lead wires as well as the platinum element. Calibrating using the same leads as in the experiment ensures lead effects are taken into account. The resistance is then calculated by dividing by a known current excitation. If Each calibrated gauge had an R^2 value of greater than 0.999, corresponding to a maximum temperature error of 0.3°C.

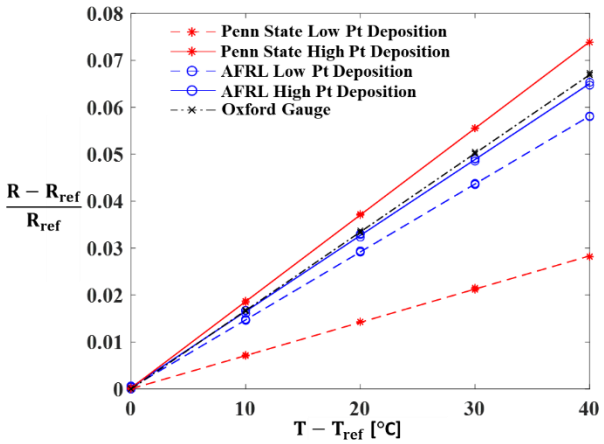

Figure 3: Calibration curve for five different thin film RTDs. The slope of the line represents the coefficient of resistance.

The calibration curves in Figure 3 represent five different gauges made from three different institutions. The sensitivity of the gauge is directly dependent on the coefficient of resistance [10], so some users find it advantageous to maximize this quantity. In this case, different levels of deposited platinum directly contribute to the coefficient of resistance: when more platinum is deposited, the coefficient of resistance increases. For deposition thicknesses greater than approximately 100 nm, quantum effects are expected to become negligible [33]. However, Table 2 shows that the coefficient of resistance for these gauges is still far from the bulk value for platinum.

Table 2: Coefficient of Resistance for Different Sensors

Manufacturer	Pt Deposition	Coefficient of Resistance (β) [°C^{-1}]
Penn State	Low (50 nm)	7.08E-4
Penn State	High (200 nm)	1.84E-3
AFRL	Low	1.45E-3
AFRL	High	1.62E-3
Oxford	--	1.67E-3
Platinum [34]	--	3.85E-3

There are two primary explanations for the discrepancies identified in Table 2 compared with the expected value for bulk platinum. First, the platinum may be improperly annealed, as temperatures higher than the polyimide decomposition point are required to achieve a fully-annealed state [35]. Second, the polyimide surface roughness may contribute. For example, platinum thin film RTDs on the order of 350nm deposited on silicon showed higher coefficients of resistance closer to the bulk values [36]. Ultimately, although sensitivity increase may be desirable, gauges with coefficients of resistance similar to Table 2 have been used successfully for several decades.

3-omega Calibration check

Because continuous-duration facilities are subject to long run times, the potential for gauge erosion over time necessitates an *in situ* calibration capability. If the gauge calibration shifts for any reason during a test, it would not be feasible to recalibrate in an oil bath before and after test campaigns due to the extended times required to remove and install necessary hardware.

To address this need, the 3-omega technique [37] states that exciting a properly-designed gauge with a sinusoidal current at frequency ω will introduce Joule heating and a corresponding temperature rise at a harmonic frequency, 2ω. In turn, this creates a voltage across the resistor that has a dominating 1ω component with a small 3ω component. By independently measuring the amplitudes of these harmonic components, Equation (1) can be applied.

$$V_{h,3\omega} = \frac{I_{h,0}^3 \beta_h}{2L\pi k} \int_0^\infty \frac{\sin^2(\eta b_h) d\eta}{(\eta b_h)^2 \sqrt{\eta^2 + q'(\omega)^2}}, \quad (1)$$

which can be solved numerically. This solution is presented in Figure 4 with a plot of thermal wavelength, given by

$$\lambda = \sqrt{\frac{k}{\rho c_p 2\omega}} = \frac{1}{|q_r|}. \quad (2)$$

To achieve accurate measurements of thermal conductivity with this method, the thermal wavelength should be less than the thickness of the material to satisfy the semi-infinite boundary condition requirement [38]. In this study, the thickness of the etched Pyralux (EP) was 50 μm. Based on these dimensions, the dashed red lines in Figure 5 illustrate the region where the linear approximation is most appropriate for the current gauge design.

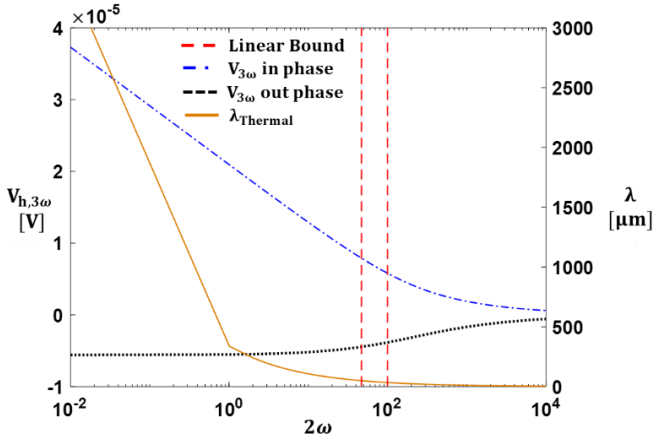

Figure 4: Numerical solution to the third harmonic of voltage solved as a function of a given heating frequency.

Simplifying Equation (1) for the linear region of the solution, Equation (3) is obtained with a log-base slope dependent upon the thermal conductivity of the polyimide and the coefficient of resistance of the heater.

$$V_{h,3\omega} = \frac{-V_{h,0}^3 \beta_h}{4\pi R_{h,0} L k} \left(\ln(2\omega) + \ln\left(\frac{b_h^2 \rho c_p}{k}\right) - 2\epsilon \right) - i \frac{V_{h,0}^3 \beta_h}{8LkR_{h,0}} \quad (3)$$

In the above equation, $V_{h,0}^3$ is measured, and $R_{h,0}$, L, and b_h are known from the gauge characterization. The thermal properties ρ,

and c_p are also considered known parameters (more details on these measurements are offered later in the paper). The frequency, ω, is controlled experimentally, therefore leaving two unknowns: β_h and k. If one of these parameters is known, then the technique can be used to solve for the other.

The technique offers two primary benefits. First, because the coefficient of resistance is known through a traditional oil bath calibration, the 3-omega method can be used to obtain thermal conductivity across a range of temperatures. Second, with knowledge of thermal conductivity as a function of temperature, the same method can be subsequently used to obtain the *in situ* coefficients of resistance, assuming the thermal properties of the substrate do not change over time. Work is currently being conducted to verify this assumption. This feature allows for the HFGs to be easily calibrated before, during, and after each measurement.

To test this theory, thermal conductivity was measured using the 3-omega method at room temperature using the gauge shown in Figure 2. The 3-omega technique was applied over a range of frequencies, and the results are reported in Figure 5. In Figure 5, the dashed lines represent the analytical solution of both the in-phase and out-of-phase signal. To obtain these curves, the thermal conductivity of the material was assumed to be a fixed known value representative of EP. Using this value as a standard, the thermal conductivity determined from the 3-omega method differed by as much as ~20%. This discrepancy is attributed to a narrow range of frequencies used to obtain the results, which will be improved by a gauge geometry change for future tests. By having a larger range of frequencies to test, a more representative thermal conductivity can be found.

Although this method is still in its preliminary stages of development for HFG use, it has been used in for decades in the nanofabrication field to characterize the thermal conductivity of thin films. Potential benefits exist by levering this established technique with HFG operation, especially in continuous-duration facilities.

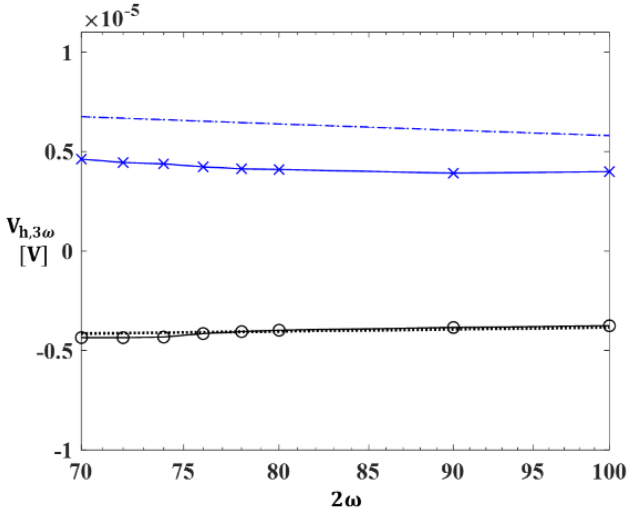

Figure 5: Results using the 3-omega method to measure thermal conductivity.

THERMAL PROPERTY DETERMINATION

The material properties required to transform measured temperature to heat flux for a double-sided type gauge are density, specific heat, and thermal conductivity, as well as the thickness of the dielectric. More precisely, the heat flux depends upon the thermal product ($\sqrt{\rho c_p k}$) and the ratio k/d. Quantifying these parameters and understanding the associated uncertainties is necessary to bound the corresponding uncertainty in the heat flux calculations. The properties presented here represent measurements of EP, and comparisons are drawn with other polyimides from previous studies.

Specific heat measurements were obtained using differential scanning calorimetry following ASTM E1269 [39]. The overall uncertainty for this method was 10%. Figure 6 shows the specific heat as a function of temperature, which exhibits a 45% variation over the range of temperatures tested and aligns well with measurements from previous studies. In previous studies, Choy [40] measured Kapton H while Kotel'nikov [41] and Lambert [42] measured generic polyimide film. In Figure 6, the value for EP reported by the manufacturer effectively represents the mean value across the selected temperature range but does not appropriately account for variations with temperature.

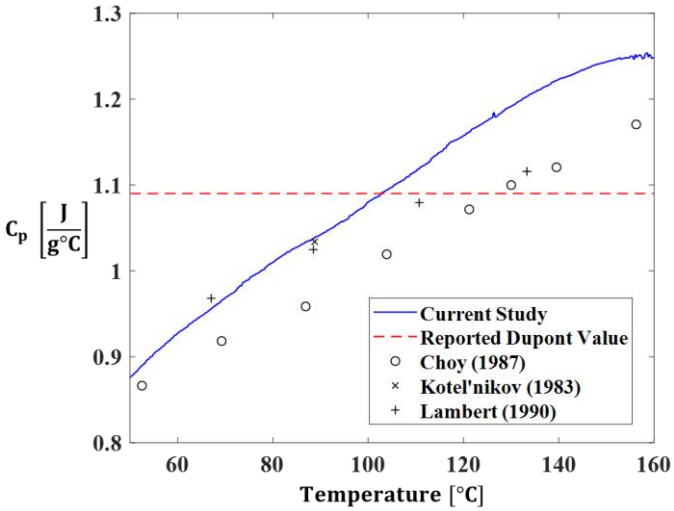

Figure 6: Specific heat as a function of temperature for EP compared with other studies.

The density of the EP was measured following ASTM D6226 – 15 [43]. This volume displacement measurement found the density to be 1510 kg/m^3 at 20°C with an accuracy of 2%. Because the thermal coefficient of expansion for these polyimide films is known with high stability, it is possible to approximate changes of density as a function of temperature using the coefficients shown in Table 3.

Because the mass of the sample remains unchanged, the density change can be correlated with volume using Equation (4) assuming isotropic expansion.

$$\frac{\Delta V}{V_{20°C}} = \frac{V_{150°C} - V_{20°C}}{V_{20°C}} = \frac{3\Delta L}{L} = 3\left[\alpha_{T_1}\Delta T_1 + \alpha_{T_2}\Delta T_2\right] \quad (4)$$

Choosing $\Delta T_1 = 70°C$ and $\Delta T_2 = 50°C$, the corresponding volume change is less than 1%, and serves as a first-order direct approximation of density variations over this temperature range,

which represents a variation much less than the other properties of interest.

Table 3: Coefficient of Thermal Expansion based upon Kapton HN

	Thermal Coefficient of Expansion [ppm/°C]	Temperature Range [°C]
α_{T_1}	17	30 - 100
α_{T_2}	32	100 - 150

Thermal conductivity measurements were collected using ISO Standard 22007-2. Three measurements were collected: Kapton HN at 23°C, EP at 23°C, and EP at 150°C, and these results are reported in Figure 7. The absolute uncertainty of the measurement is 5%, and the relative standard deviation was less than 2.3%. Although only two points were measured for EP, the thermal conductivity of the samples varied by more than 27% over the temperature range of interest.

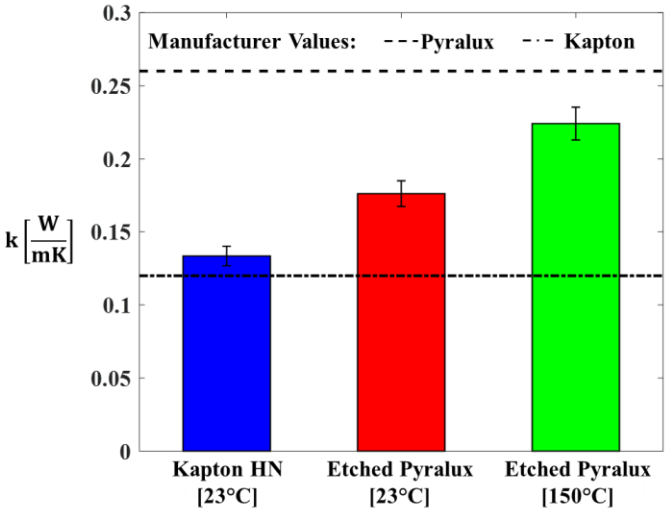

Figure 7: Thermal conductivity measurements for EP as a function of temperature.

After each thermal property was individually characterized, the thermal product ($\sqrt{\rho c_p k}$) was examined. Table 4 compares the present study with measurements at two temperatures to previously published data from AFRL [27], Oxford [23,24], MIT [3], and VKI [32] as well as manufacturer-reported specifications [44–46]. Although this table shows a wide range of values, this spread is not unexpected. Each institution characterized their own materials, and the methods for quantifying thermal properties varied between studies. In the studies from VKI and Oxford, the material the gauge was mounted upon was taken into account, which is why Table 4 has multiple studies or values from the same institution. Details about the methods can be obtained from the individual references. Although the dielectric was always a polyimide, manufacturers and batch-to-batch variations contribute noticeably to the result. Based on this observation, it is increasingly important for users to regularly measure the thermal properties of the dielectric for each sensor build to obtain high-quality heat flux measurements.

Beyond the discrete results provided for the present study in Table 4, the combination of measured properties over a range of temperatures yields thermal product for all temperatures between 50°C and 100°C. In this case, the thermal conductivity was only measured at two temperatures, but a linear approximation between those two points is appropriate [40]. The results in Figure 8 are presented as a variation normalized by their mean values across the range of measurements. From this graph, it is easy to see that the specific heat contributes the most to the change in thermal product followed by the thermal conductivity. The density variations are an order of magnitude less than the other two parameters.

Based on the variations identified in Figure 8, it is important to quantify thermal properties at the temperature of operation to reduce errors. This importance increases for continuous-duration facilities that may have a larger variance of local gauge operating temperatures. In Table 4, Oxford, MIT, and VKI implicitly obtained thermal properties as lumped parameters, but discussions of varying temperatures were not included. In contrast, individual parameter measurements in the present study provide an inherent ability to control the temperature.

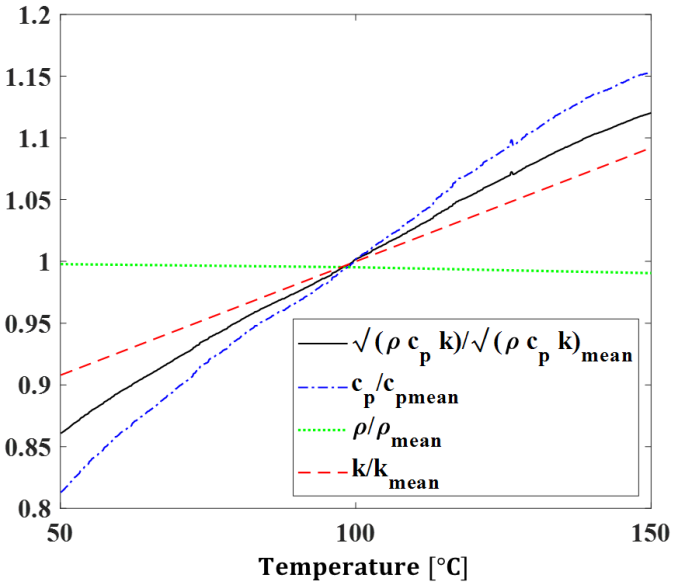

Figure 8: Variation of thermal properties as a function of temperature, normalized by mean value over temperature range.

ERROR SENSITIVITY ANALYSIS

Although this study considers both the single- and double-sided gauges, double-sided gauges must be used in a continuous-duration facility because the backside (metal) temperature will not fulfill a semi-infinite assumption. For this reason, the subsequent error sensitivity analysis was completed for a double-sided gauge only.

The uncertainty analysis was completed using a perturbation method in conjunction with Oldfield's Impulse Response Theory (IRT) toolbox [48]. This toolbox takes the temperature signals from the gauge, T_{top} and T_{bot}, as well as the material properties as inputs. The output is the corresponding heat flux. Since the thermal properties are a function of temperature, it is advantageous to quantify the uncertainty in the output, q, for thermal properties at different temperatures.

To this point, calculated heat flux has been introduced as a function of the top and bottom gauge temperatures, the thermal product, and the thermal conductivity over the thickness of the substrate. As shown in the last section, the thermal conductivity and specific heat are direct functions of temperature. To obtain accurate measurements, the temperature of the EP during test operation must be known, and the operating temperature must fall within the temperature range over which the thermal properties were characterized. To illustrate the importance of these steps, a synthetic test signal is considered whose data are captured at an EP temperature of 100°C and creates a constant heat flux of 50,000 W/m^2 as shown in Figure 9. The temperature traces come from analytical solutions while the thermal properties come from experimental conditions. By using analytical temperature traces, the influence of thermal properties can be isolated from signal noise and an imperfect experimental set-up.

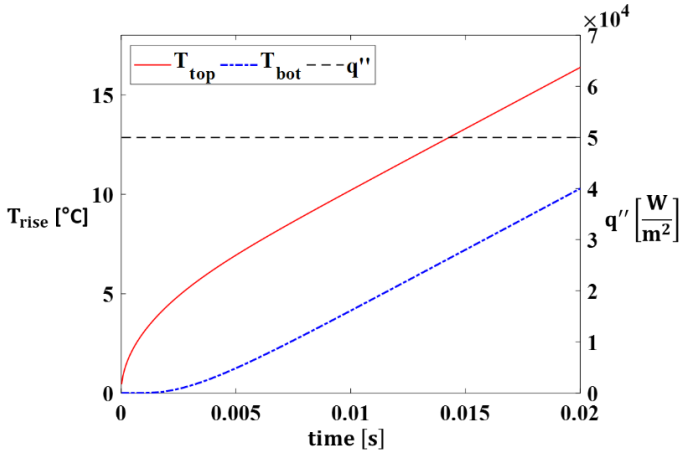

Figure 9: Analytical temperature traces from two sides of a double-sided gauge corresponding to a constant heat flux.

To understand the influence of thermal property variations with temperature on calculated heat flux, the same temperature traces are considered (i.e., with a substrate temperature of 100°C), but the results were processed (with IRT) using thermal properties of the EP substrate quantified at temperatures different from the operating temperature. Following this process, Figure 10 shows the percent error, ε, introduced by variations of thermal properties with temperature, defined by:

$$\varepsilon = \left| \frac{\overline{q_{T_{op}}} - \overline{q_{T_{prop}}}}{\overline{q_{T_{prop}}}} \right| \times 100\%, \qquad (5)$$

Table 4: Comparison of Thermal Properties from Various Studies Used to Calculate Heat Flux through Thin Polyimide Films.

Institution	Ref	Material	ρ $\left[\frac{kg}{m^3}\right]$	c_p $\left[\frac{J}{kgK}\right]$	k $\left[\frac{W}{mK}\right]$	$\sqrt{\rho c_p k}$ $\left[\frac{J}{Km^2 s^{0.5}}\right]$	% Diff Relative to T_{prop}=50°C	% Diff Relative to T_{prop}=150°C	Uncertainty $\sqrt{\rho c_p k}$
Present Study [50°C]	--	Etched Pyralux	1510	876	0.19	496	--	30.85%	5.89%
Present Study [150°C]	--	Etched Pyralux	1510	1243	0.22	649	30.85%	--	6.25%
Air Force (2011) [23°C]	[27]	Kapton HN	1410	1058	0.18	518	4.44%	20.18%	6.52%
Oxford (1999)	[24]	Upilex	--	--	--	495	0.00%	23.73%	4.20%
Oxford (1986)	[23]	Kapton HN	--	--	--	560	12.90%	13.71%	--
MIT (1985)	[3]	Kapton HN	--	--	--	575	15.93%	11.40%	5.00%
VKI (2002)	[32]	Upilex	--	--	--	699-731	47.37%	12.63%	8.80%
Dupont	[47]	Etched Pyralux	1430	1089	0.26	636	28.23%	2.00%	--
DuPont	[45]	Kapton HN	1420	1090	0.12	431	13.10%	33.59%	--
UBE	[46]	Upilex-S	1470	1130	0.29	649	30.85%	0.00%	--

The abscissa in Figure 10 is denoted as T_{op} - T_{prop} where T_{op} is the operating temperature of the gauge and T_{prop} is the evaluation temperature of the thermal properties. Based on Figure 10, the operating temperature must be within ±10°C of the temperature at which properties were measured to achieve a corresponding error less than 3%. As a corollary to this statement, if a discrepancy between operating temperature and characterization temperature of 50°C occurs, an error of up to 14% may be introduced. This error arises because the temperature traces used to create the constant heat flux will alter the shape of the resulting heat flux when processed with different thermal properties. As the trend of thermal product with temperature shown in Figure 10 is approximately linear, the corresponding influence on error propagated through the processing algorithm yields a pattern in Figure 10 that is approximately symmetric. The results in Figure 10 were also evaluated for different levels of mean heat flux and different operating temperatures, yielding negligible differences on the magnitude or trend of error as a function of temperature.

In this assessment, the error quantified in Figure 10 is independent of the accuracy of the measured properties themselves. Using information from the previous sections, the uncertainties of thermal conductivity (k), specific heat (c_p), and density (ρ) are 5%, 10%, 2%, respectively. Other factors include uncertainty of measured temperature, dielectric thickness (believed to be 10% [44]), and calibration coefficient of resistance of the RTD (0.5%). Assuming that the thermal properties are known for the temperature at which data is recorded (i.e., independent of the errors introduced in Figure 10), the overall effect on the calculation of heat flux from the above uncertainties is approximately 8%, and was calculated using a perturbation method [49]. A combination of these relative errors would be applied for each individual application to calculate a representative overall uncertainty.

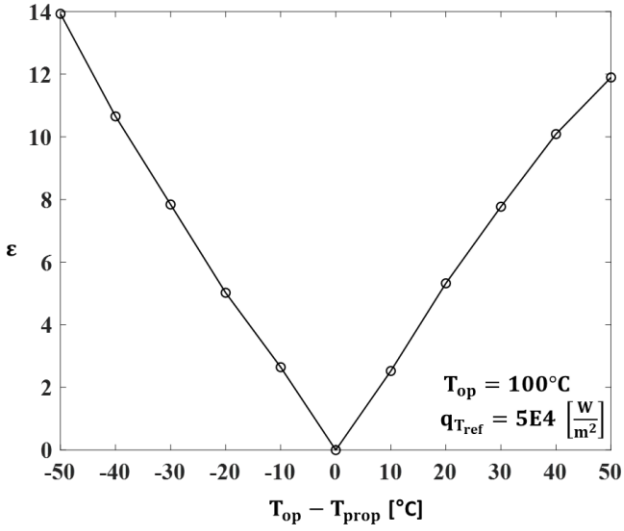

Figure 10: Error in the quantified heat flux based on a temperature difference between gauge operating temperature and thermal property evaluation temperature.

STEADY FACILITY POST PROCESSING

Although many post processing schemes for double-sided heat flux gauges exist, the impulse response theory (IRT) introduced by Oldfield [48] is widely used for its low numerical error and computational efficiency. However, this method assumes the measurements start from a zero condition, dictating an inherent settling time that appears when processing data beginning from a steady operating condition. This settling time is derived from the Laplace transform and one-sided z-transform both starting at t = 0 in the IRT analysis. Therefore, to apply this processing technique for continuous-operation facilities, the settling time and the associated errors must be quantified by comparing the analytical and numerical solution. Although the error has been studied previously for a step change in heat flux (i.e., short-duration blow-down tests), a step change does not correlate well to continuous-duration facility operation. To more accurately represent the conditions in a continuous duration flow facility, synthetic temperature traces were created which correspond to a sinusoidal heat flux around a known mean value, and these signals were filtered using Oldfield's toolbox for comparison with the analytical solution. Starting with the boundary condition for heat flux experienced by the gauge,

$$q''(t) = -k\frac{\partial T}{\partial x}\Big|_{x=0} = Q_{mean} + Q_0 \sin(\varpi t)\,, \qquad (6)$$

where x = 0 is the top (air side) of the gauge and x = d at the back (metal side), an analysis was performed for a sensor neglecting glue layers and protective layers on top of the gauge.

Synthetic temperature profiles for the top and bottom of the gauge were found solving the unsteady conduction equation. A full analysis of the analytical solution can be found in previous work [3]. Figure 11 shows the result comparing the analytical solution with processed data using the IRT method for a single sinusoidal frequency, ϖ. In Figure 11, the analytical solution is represented by the dashed line. For times at the beginning of the processed data window, there is a discrepancy between the heat flux calculated through Oldfield's IRT method (solid line) and the analytical solution. Because the IRT solution asymptotically approaches the analytical solution, the time at which one full period is within 1% of the analytical solution is denoted $t_{\varepsilon 1}$.

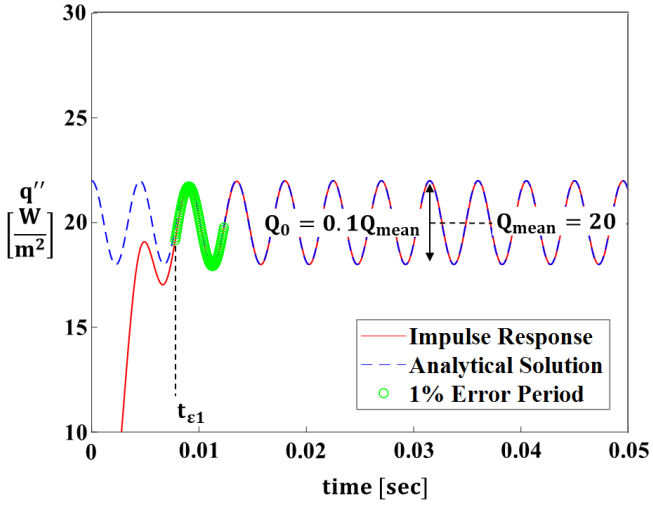

Figure 11: Impulse response processing for a sinusoid.

Following the procedure outlined in Figure 11, a series of cases were tested over a frequency range from 0-50 kHz (covering several harmonics of potential blade passing frequencies).The Q_0 and Q_{mean} values were varied as seen in Table 5. These were chosen to account for different fluctuation levels in the signal.

For all test cases, the settling time to reach an error below 1% was less than 0.01 seconds over the entire range of frequencies. These results, shown in Figure 12, are a function of the ratio of the amplitude to the mean value, with an inverse relationship between heat flux amplitude and calculated settling time. Phase lag and RMS error were also calculated with influences less than 0.5% for all values tested. Because all the error metrics tested were found to be less than 0.5% after the settling time, this method of data processing can be applied for continuous-duration facilities if the user collects more data than necessary and identifies that an initial portion must be removed to account for the settling time associated with the processing technique.

Table 5: Parameters Tested for IRT under Steady Operation.

Parameter		Tested Values
ϖ	[kHz]	0-50
Q_{mean}	$\left[\frac{W}{m^2}\right]$	[2, 20, 2×10^5]
$\frac{Q_0}{Q_{mean}}$	$\left[\frac{W}{m^2}\right]$	[0.01, 0.1, 0.5]

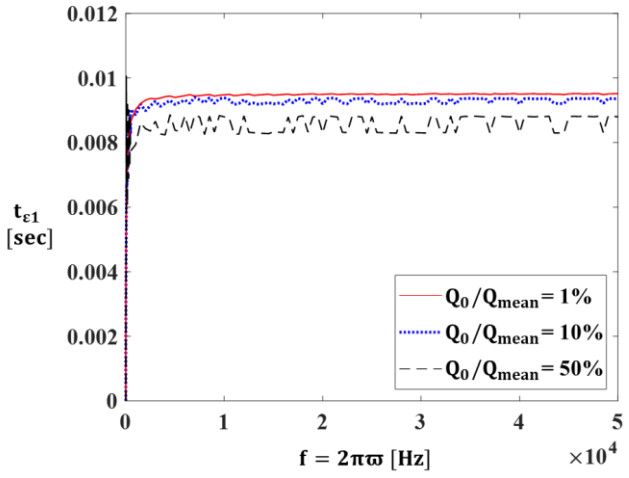

Figure 12: Correction time for 1% error vs heating frequency.

IMPINGING JET EXPERIMENTAL SETUP

After characterizing the individual properties of the gauges, a shutter-rig-type experiment was setup to test the whole gauge at the device level. This test apparatus consists of a heat gun mounted at a fixed distance from an HFG sensor. The heat gun was experimentally characterized as a function of device control settings (outlet temperature and flow level) with the use of a pitot-static probe and thermocouple to measure the exit conditions of the device. Through this process, three Reynolds numbers based on nozzle diameter, Re_D, were selected for assessment: 5×10^3, 10×10^3, and 12×10^3.

To quantify the heat flux from the heat gun, a Vatell Heat Flux Microsensor (HFM) was mounted at a spacing of 4D from the outlet of the heat gun, as shown in Figure 13. This sensor has an uncertainty of 5% and was used as the reference in this study [50], and the spacing was chosen to compare with literature [51]. Results from the impinging jet at all Re_D were found to be within 10% of values for Re_D.= 10×10^3 and Re_D.= 12×10^3 reported in the literature study.

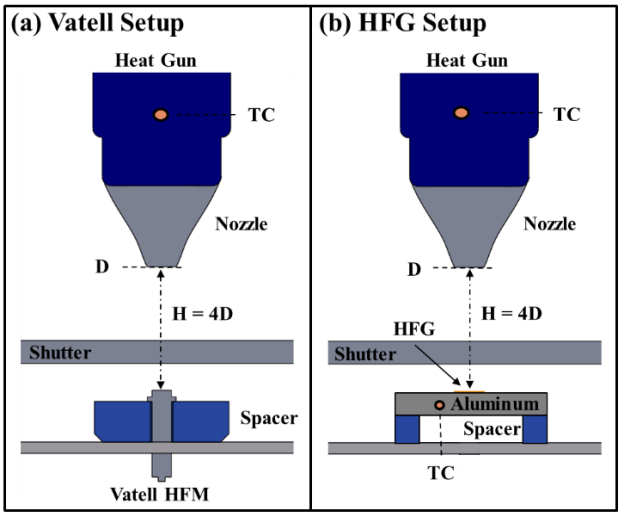

Figure 13: Diagram of experimental setup for shutter rig tests where (a) shows the reference gauge and (b) shows how the HFGs were mounted.

COMPARISON OF GAUGE PERFORMANCE

Three different thin film heat flux gauges were used under the shutter rig. The first was a double-sided thin film heat flux gauge manufactured by AFRL. The second and third were a single-sided gauge manufactured at Penn State and Oxford. Note that because of the experimental setup, both double- and single-sided gauges could be used. Although double-sided gauges must be used in a steady facility, for a transient jet, both are applicable.

Each gauge was excited using a current amplitude selected to yield a voltage drop across the resistor of 0.25 V at room temperature. Because the single-sided gauges require accurate thermal properties of the material onto which the gauges are mounted, the gauges were adhered onto an aluminum block whose thermal properties were measured using the same techniques outlined above. The aluminum block was instrumented with thermocouples to quantify the backside temperature of the block, as well as the temperature near the surface to compare to the thin film RTDs. When accounting for the uncertainty in the second layer thermal properties, the uncertainty in the measured heat flux from a single-sided PSU gauges is 10%, calculated by using the upper and lower bound for the thermal properties to determine the heat flux and comparing the difference.

These results, shown in Figure 14, were averaged over 0.3 seconds of steady data after the shutter was released (sampled at 5 kHz). Also in Figure 14 are values from Goldstein et al who measured the heat flux from an impinging jet over a similar range

of Re_D using a temperature sensitive liquid crystal technique (LCT) [51]. For each gauge, the heat flux was calculated using the thermal properties provided by the respective institution and reported in Table 4. Because the thermal properties of the Penn State gauge were known for a range of temperatures, the mean temperature of the sensor over the 0.3 second averaging window was used to calculate the heat flux, which was not possible with the single values from other institutions. To calculate the thickness of the sample, a three-dimensional microscope was used with a resolution of 4 μm. Combining this information, error bars in the figure were calculated using the quoted uncertainty from each institution.

Overall, the gauge in closest agreement with the reference was Penn State. Because all three gauges were calibrated and excited with the same system, the errors between the gauges must be from the thermal properties used to process the data. Since the Penn State property determination came from a piece of EP near where the gauge was built, it was potentially more representative of the dielectric than the values quoted by the other institutions. For this reason, this specific gauge read closer to the commercially available gauge. This statement reiterates the importance of quantifying thermal properties for each set of gauge builds.

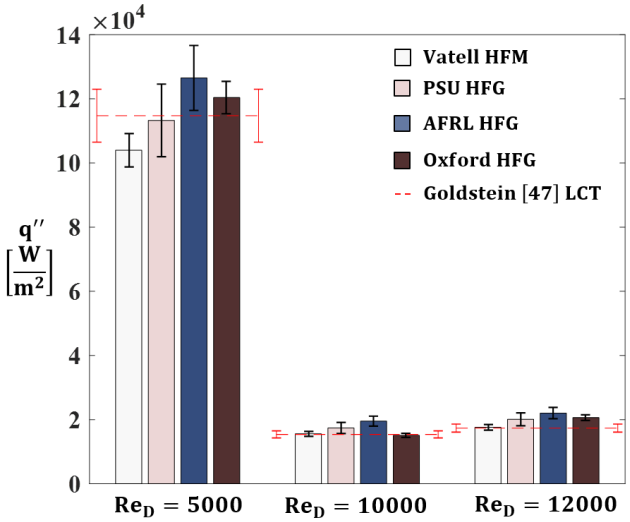

Figure 14: Comparison of gauges under impinging jet using shutter rig apparatus with literature values.

CONCLUSIONS

This study addresses the development and implementation of thin film heat flux gauges specific to a continuous-duration test facility, such as the Steady Thermal Aero Research Turbine Laboratory at Penn State. The fabrication of the gauges has been outlined and shown to have alignment within 5 microns which is critical to the orthogonal 1D assumption in a steady facility. Although the fabrication is an important step, gauge deterioration is a major concern for steady-operating facilities.

To address this concern, unique calibration procedures involving the 3-omega method show utility as a method to assess gauge deterioration and perform *in situ* calibration verifications. This method enables more frequent calibrations, thereby lowering uncertainty in the measurements associated with long run times.

Thermal property determination, which represents a significant contribution of error in heat flux measurements, was addressed by independently measuring the density, specific heat, and thermal conductivity over a range of temperatures. These measurements showed an overall thermal product variation of more than 30% over the range of temperatures studied. Using this information an analytical solution to a step change in heat flux was used to determine the error in the heat flux measurement introduced by evaluating heat flux with thermal properties quantified at a temperature different from the sensor operating temperature through Impulse Response Theory. Based on these measurements with polyimide films, thermal properties should be measured within 10°C of desired test conditions to maintain a propagated error less than 3%.

For post processing, the IRT method was used for its computational efficiency. Post processing errors from the IRT method were calculated using an analytical solution to a sinusoidal heat flux. Over a range of frequencies, the associate settling time to achieve a processed error less than 1% is less than 0.01 second, and the settling time is independent of mean heat flux level. The RMS and mean value errors for the method were also found to create less than a 0.5% error over all frequencies.

Finally, the mean heat flux from an impinging jet was measured using thin film heat flux gauges from Penn State, AFRL, and Oxford. All gauges show agreement with a defined standard that was within their uncertainty over all conditions tested. Because the accuracy of these gauges depends on thermal property determination, the importance of correct thermal property determination is shown exemplifying that to obtain accurate measurements, thermal properties must be checked often for the specific polyimide beneath the gauge.

Beyond steady facilities, the process outlined in this paper shows the course of HFG implementation in any steady environment, including gas turbine engines themselves. Although the fabrication techniques must advance before such implementation, the process of calibration, thermal property determination, and data post-processing can stay the same to those outlined in this paper.

ACKNOWLEDGMENTS

The authors would like to recognize and thank Pratt & Whitney and the U.S. Department of Energy National Energy Technology Laboratory under Award Number DE-FE0025011 for supporting research presented in this paper. The authors also thank the staff at Penn State's Nanofabrication Lab. This work would not have been possible without their knowledge, specifically Michael Labella, Kathy Gehoski, and Ted Gehoski. Appreciation is also given to Prof. Martin Oldfield whose Impulse Response Method was used to process the heat flux data and who gave insight to the inherent settling time that goes with the process. Finally, the authors are grateful to Carlos Vargas Venegas who pioneered the thin film thermal property techniques at Penn State and Brian Siroka, who ran many shutter rig tests to obtain some of the data presented in this work.

This report was prepared as an account of work sponsored by an agency of the United States Government. Neither the United States Government nor any agency thereof, nor any of their employees, makes any warranty, express or implied, or assumes any legal liability or responsibility for the accuracy,

completeness, or usefulness of any information, apparatus, product, or process disclosed, or represents that its use would not infringe privately owned rights. Reference herein to any specific commercial product, process, or service by trade name, trademark, manufacturer, or otherwise does not necessarily constitute or imply its endorsement, recommendation, or favoring by the United States Government or any agency thereof. The views and opinions of authors expressed herein do not necessarily state or reflect those of the United States Government or any agency thereof.

REFERENCES

[1] Jones, T. V., and Schultz, D. L., 1973, "Heat-Transfer Measurements In Short-Duration Hypersonic Facilities," *Proc. 4th Natl. UK Heat Transf. Conf.*

[2] Chana, K., Cardwell, D., and Jones, T., 2013, "A Review of the Oxford Turbine Research Facility," *Proc. ASME Turbo Expo 2013*, pp. 1–17.

[3] Epstein, A. H., Guenette, G. R., Norton, R. J. G., and Yuzhang, C., 1986, "High-Frequency Response Heat-Flux Gauge," *Rev. Sci. Instrum.*, **57**(4), pp. 639–649.

[4] Mathison, R. M., Wishart, M. B., Haldeman, C. W., and Dunn, M. G., 2012, "Temperature Predictions and Comparison With Measurements for the Blade Leading Edge and Platform of a 1 1/2 Stage Transonic HP Turbine," *J. Turbomach.*, **134**(1), p. 011016.

[5] Iliopoulou, V., Dénos, R., Billiard, N., and Arts, T., 2004, "Time-Averaged and Time-Resolved Heat Flux Measurements on a Turbine Stator Blade Using Two-Layered Thin-Film Gauges," *J. Turbomach.*, **126**(4), p. 570.

[6] Nasir, S., Carullo, J. S., Ng, W.-F., Thole, K. A., Wu, H., Zhang, L. J., and Moon, H. K., 2009, "Effects of Large Scale High Freestream Turbulence and Exit Reynolds Number on Turbine Vane Heat Transfer in a Transonic Cascade," *J. Turbomach.*, **131**(2), p. 021021.

[7] Clark, J. P., Polanka, M. D., Meininger, M., and Praisner, T. J., 2006, "Validation of Heat-Flux Predictions on the Outer Air Seal of a Transonic Turbine Blade," *J. Turbomach.*, **128**(3), p. 589.

[8] Anthony, R. J., Jones, T. V., and LaGraff, J. E., 2005, "High Frequency Surface Heat Flux Imaging of Bypass Transition," *J. Turbomach.*, **127**(2), p. 241.

[9] Dunn, M., and Mathison, R., 2013, "History of Short-Duration Measurement Programs Related to Gas Turbine," *ASME Turbo Expo 2013: Turbine Technical Conference and Exposition*, San Antonio.

[10] Epstein, A. H., Guenette, G. R., and Norton, R. J. G., 1985, *The Design of the MIT Blowdown Turbine Facility*.

[11] Sieverding, C. H., and Arts, T., 1992, "The VKI Compression Tube Annular Cascade Facility CT3," *Int. Gas Turbine Aeroengine Congr. Expo. Col. Ger. June 1-4, 1992*, pp. 1–10.

[12] Dunn, M. G., George, W. K., Rae, W. J., Woodward, S. H., Moller, J. C., and Seymour, P. J., 1986, "Heat Flux Measurements for the Rotor of a Full-Stage Turbine: Part {II} - Description of Analysis Technique and Typical Time Resolved Measurements," *Trans. ASME, J. Turbomach.*, **108**(July 1986), pp. 98–107.

[13] Guenette, G. R., Epstein, a. H., Giles, M. B., Haimes, R., and Norton, R. J. G., 1989, "Fully Scaled Transonic Turbine Rotor Heat Transfer Measurements," *J. Turbomach.*, **111**(January), p. 1.

[14] Haldeman, C. W., and Dunn, M. G., 2003, "Heat Transfer Measurements and Predictions for the Vane and Blade of a Rotating High-Pressure Turbine Stage," *ASME Conf. Proc.*, **2003**(36886), pp. 591–600.

[15] Kahveci, H. S., Haldeman, C. W., Mathison, R. M., and Dunn, M. G., 2012, "Heat Transfer for the Film-Cooled Vane of a 1-1/2 Stage High-Pressure Transonic Turbine—Part II: Effect of Cooling Variation on the Vane Airfoil and Inner End Wall," *J. Turbomach.*, **135**(2), p. 021028.

[16] Guo, S. M., Spencer, M. C., Lock, G. D., Jones, T. V., and Harvey, N. W., 1995, "The Application of Thin Film Gauges on Flexible Plastic Substrates to the Gas Turbine Situation," *IGTI Turbo Expo*, **95-GT-357**(Ccc).

[17] Haldeman, C. W., Dunn, M. G., Barter, J. W., Green, B. R., and Bergholz, R. F., 2004, "Aerodynamic and Heat-Flux Measurements With Predictions on a Modern One and 1/2 Stage High Pressure Transonic Turbine," *ASME Conf. Proc.*, **2004**(41685), pp. 439–450.

[18] Polanka, M. D., Hoying, D. A., Meininger, M., and MacArthur, C. D., 2002, "Turbine Tip and Shroud Heat Transfer and Loading: Part A — Parameter Effects Including Reynolds Number, Pressure Ratio, and Gas to Metal Temperature Ratio," *Vol. 3 Turbo Expo 2002, Parts A B*, **125**(January 2003), pp. 219–230.

[19] Polanka, M. D., Clark, J. P., White, A. L., Meininger, M., and Praisner, T. J., 2003, "Turbine Tip and Shroud Heat Transfer and Loading: Part B — Comparisons Between Prediction and Experiment Including Unsteady Effects," *Vol. 5 Turbo Expo 2003, Parts A B*, (1984), pp. 691–702.

[20] Chana, K. S., and Jones, T. V., 2003, "An Investigation on Turbine Tip and Shroud Heat Transfer," *J. Turbomach.*, **125**(3), p. 513.

[21] Hager, J. M., Simmons, S., Smith, D., Onishi, S., Langley, L. W., and Diller, T. E., 1991, "Experimental Performance of a Heat Flux Microsensor," *J. Eng. Gas Turbines Power*, **113**(2), p. 246.

[22] Ewing, J., Gifford, A., Hubble, D., Vlachos, P., Wicks, A., and Diller, T., 2010, "A Direct-Measurement Thin-Film Heat Flux Sensor Array," *Meas. Sci. Technol.*, **21**(10).

[23] Doorly, J. E., and Oldfield, M. L. G., 1986, "New Heat Transfer Gages for Use on Multilayered Substrates," *J. Turbomach.*, **108**(1), p. 153.

[24] Piccini, E., Guo, S. M., and Jones, T. V., 2000, "The Development of a New Direct-Heat-Flux Gauge for Heat-Transfer Facilities," *Meas. Sci. Technol.*, **11**(4), pp. 342–349.

[25] Duan, F. L., Li, J., Gao, J., Ding, G., and Cao, X., 2018, "Integrated Fabrication of High Temperature MEMS Sensor on Aero Engine Turbine Blade," *J. Thermophys. Heat Transf.*, **xx**(xx), pp. 8–11.

[26] Hodak, M. P., 2010, "Quantification of Fourth Generation Kapton Heat Flux Gauge Calibration Performance," Ohio State University.

[27] Anthony, R. J., Clark, J. P. ., Kennedy, S. W., Finnegan, J. M., Johnson, D., Hendershot, J., and Downs, J., 2011, "Flexible Non-Intrusive Heat Flux Instrumentation on the Afrl Research Turbine," *Proceedings of ASME TURBO EXPO 2011*, pp. 1–11.

[28] Collins, M., Chana, K., and Povey, T., 2015, "New Technique for the Fabrication of Miniature Thin Film Heat Flux Gauges," *Meas. Sci. Technol.*, **26**(2).

[29] Doorly, J. E., and Oldfield, M. L. G., 1987, "The Theory of Advanced Multi-Layer Thin Film Heat Transfer Gauges," *Int. J. Heat Mass Transf.*, **30**(6), pp. 1159–1168.

[30] De Cuyper, T., Fossaert, G., Collet, O., Broekaert, S., Chana, K., De Paepe, M., and Verhelst, S., 2015, "Calibration of a TFG Sensor for Heat Flux Measurements in a S.I. Engine," *SAE Int. J. Engines*, **8**(4), pp. 2015-01-1645.

[31] Zilles, D., 1999, "The Effect of Non-Isothermal Wall Boundary Temperature on Convective Heat Flux over a Flat Plate," The Ohio State University.

[32] Billiard, N., Iliopoulou, V., Ferrara, F., and Dénos, R., 2002, "Data Reduction and Thermal Product Determination for Single and Multi-Layered Substrate Thin-Film Gauges," *16th Symp. Meas. Tech. Transonic Supersonic Flow Cascades Turbomachines*, (September), pp. 1–9.

[33] Lacy, F., 2011, "Developing a Theoretical Relationship between Electrical Resistivity, Temperature, and Film Thickness for Conductors," *Nanoscale Res. Lett.*, **6**(1), pp. 1–26.

[34] WIKA, 2014, *Callendar-Van Dusen Equations for the Calibration of Platinum Resistance Thermometers*.

[35] Zhang, J., Nagao, Y., Kuwano, S., and Ito, Y., 1997, "Microstructure and Temperature Coefficient of Resistance of Platinum Films," *Japanese J. Appl. Physics, Part 1 Regul. Pap. Short Notes Rev. Pap.*, **36**(2), pp. 834–839.

[36] Kreider, K. G., Ripple, D. C., and Kimes, W. A., 2009, "Thin-Film Resistance Thermometers on Silicon Wafers," *Meas. Sci. Technol.*, **20**(4), pp. 1–18.

[37] Cahill, D. G., 1990, "Thermal Conductivity Measurement from 30 to 750 K: The 3ω Method," *Rev. Sci. Instrum.*, **61**(2), pp. 802–808.

[38] de Koninck, D., 2008, "Thermal Conductivity Measurements Using the 3-Omega Technique: Application to Power Harvesting Microsystems," *McGill Univ. thesis*.

[39] American Society for Testing and Materials (ASTM®), 2011, "ASTM E1269 - Standard Test Method for Determining Specific Heat Capacity by Differential Scanning," *ASTM Stand.*, **i**, pp. 1–6.

[40] Choy, C. L., Leung, W. P., and Ng, Y. K., 1987, "Thermal Diffusivity of Polymer Films by the Flash Radiometry Method," *J. Polym. Sci. Part B Polym. Phys.*, **25**(9), pp. 1779–1799.

[41] Kotel'nikov, G. V., and Sidorovich, A. V., 1983, "Microcalorimeter Type DSM-2M for Use in the Study of Polymers," *Polym. Sci. U.S.S.R.*, **25**(12), pp. 3053–3059.

[42] Brunco, D. P., Thompson, M. O., Otis, C. E., and Goodwin, P. M., 1992, "Temperature Measurements of Polyimide during KrF Excimer Laser Ablation," *J. Appl. Phys.*, **72**(9), pp. 4344–4350.

[43] ASTM, 1998, "Standard Test Method for Open-Cell Content of Rigid Cellular Plastics by the Air," **94**(May 1994), pp. 1–6.

[44] DuPont, *Kapton Gerneal Specifications*.

[45] DuPont, 2011, "DuPont Kapton HN Technical Data Sheet," **5213**, pp. 1–4.

[46] UBE Europe, 2013, *Upilex-S*.

[47] DuPont, 2018, "Personal Communication."

[48] Oldfield, M. L. G., 2008, "Impulse Response Processing of Transient Heat Transfer Gauge Signals," *J. Turbomach.*, **130**(2), p. 021023.

[49] Moffat, R. J., 1982, "Contributions to the Theory of Single-Sample Uncertainty Analysis," *J. Fluids Eng.*, **104**(2), p. 250.

[50] Vatell Corporation, 2015, *HFM-6, HFM-7, & HFM-8*.

[51] Goldstein, R. J., and Franchett, M. E., 1988, "Heat Transfer From a Flat Surface to an Oblique Impinging Jet," *J. Heat Transfer*, **110**(1), p. 84.